LETTER

Hydrodynamics of contraction-based motility in a compressible active fluid

View the article online for updates and enhancements.

Hydrodynamics of contraction-based motility in a compressible active fluid

G. Negro[1], A. Lamura[2], G. Gonnella[1] and D. Marenduzzo[3]

[1] *Dipartimento di Fisica, Universitá degli studi di Bari and INFN, Sezione di Bari - Via Amendola 173,*
70126 Bari, Italy
[2] *Istituto Applicazioni Calcolo, CNR - Via Amendola 122/D, 70126 Bari, Italy*
[3] *SUPA, School of Physics and Astronomy, University of Edinburgh - Peter Guthrie Tait Road,*
Edinburgh EH9 3FD, UK

Abstract – Cell motility is crucial to biological functions ranging from wound healing to immune response. The physics of cell crawling on a substrate is by now well understood, whilst cell motion in bulk (cell swimming) is far from being completely characterized. We present here a minimal model for pattern formation within a compressible actomyosin gel, in both 2D and 3D, which shows that contractility leads to the emergence of an actomyosin droplet within a low density background. This droplet then becomes self-motile for sufficiently large motor contractility. These results may be relevant to understand the essential physics at play in 3D cell swimming within compressible fluids. We report results of both 2D and 3D numerical simulations, and show that the compressibility of actomyosin plays an important role in the transition to motility.

Introduction. – Understanding how cells move around their surroundings is a fascinating question that has gained much attention in the recent past. Answering this question would constitute a substantial step-forward in dissecting the fundamental mechanisms underlying biomedical problems like wound-healing and tissue self-assembly during embryogenesis [1]. Spontaneous movement and deformation are physically driven by the cell cytoskeleton. The cytoskeleton consists of protein filaments and motors which constantly consume chemical energy (ATP) and convert it to work. In particular, actin filaments interact with myosin motors to generate contraction forces in the cell, which can drive cell motion and division [2–7].

Most of the research has focused, both experimentally and theoretically, on cells migration on a two-dimensional substrate (*crawling*) [8–11], mainly because such experimental systems are easily accessible hence this motion is more readily observable. These studies have stimulated the development of theories which now provide a detailed outline of some basic migration mechanisms, including the formation of *lamellipodia* arising from *actin* polymerization at the cell front, adhesion-mediated traction, and

actomyosin contractility. The crawling motility mode requires actin cytoskeleton to be anchored to the substrate throughout *focal adhesions*, that are clusters of transmembrane proteins binding to the substrate [8].

However some cells, such as breast tumor cells, can also "swim" in a straight line inside a 3D tissue or a polymeric fluid [12]. Unlike cell crawling, in this case there is no solid surface present, and no cellular protrusion reminiscent of a lamellipodium (the cell shape instead remains roughly spherical). The lack of protrusions suggests that actin polymerisation may not be crucial for 3D cell swimming. Indeed, myosin motors contraction is believed to be the sole responsible for cell polarisation and motility [12]: together with some experiments on tumour cells [13], this observation suggests that cell swimming may be primarily driven by myosin activity.

Models of contraction-induced motility have been proposed in refs. [5–7,14]. All these considered the case of an active droplet moving inside a simple (Newtonian) and passive outer fluid. In some cases, the material inside the droplet was an active liquid crystal, in which case the onset of motility required rectifications of orientational splay fluctuations of an order parameter linked to

actin polarisation [5,14]. In this work instead we study by lattice Boltzmann simulations a simpler, single-phase, compressible actomyosin system, where a high density droplet (actomyosin blob) simply emerges due to active contraction. For sufficiently strong activity, we find that the self-assembled droplet swims inside a low density actomyosin background. The setup we consider could be studied experimentally with quasi-2D or 3D compressible actomyosin suspensions. Additionally, once the droplet emerges, the system is approximately equivalent to an active compressible actomyosin droplet swimming inside a generic compressible and passive fluid (as the density of motors in the background is very small). Therefore, our results can be qualitatively compared to experiments studying the motion of cells or cell extracts within polymeric or viscoelastic fluids. Indeed, we show that the hydrodynamic flows in the region outside the droplet are reminiscent of the flow of matrigel[1] surrounding swimming cells.

Model. – We model an actin suspension as a compressible fluid with local density ρ, and myosin via its concentration field ϕ. Rather than considering the case in which actin is enclosed in a droplet [7], we study a single-fluid set-up with a compressible actin gel initially uniform in the simulation domain. The dynamical equation of motion for the actin density ρ is the continuity equation

$$\partial_t \rho + \partial_\alpha \rho v_\alpha = 0, \qquad (1)$$

with v_α the velocity of the actin fluid. The latter obeys the following Navier-Stokes momentum balance equation:

$$\partial_t \rho v_\alpha + \partial_\beta (\rho v_\alpha v_\beta) = F_\alpha^{\text{int}} + F_\alpha^{\text{active}} \\ + F_\alpha^{\text{interface}} + F_\alpha^{\text{viscous}}, \qquad (2)$$

where $F_\alpha^{\text{viscous}} = \partial_\beta[\eta(\partial_\beta v_\alpha + \partial_\alpha v_\beta)]$ is the usual viscous term, with η shear viscosity of the fluid. The term

$$F_\alpha^{\text{int}} = -\partial_\alpha P^i + \partial_\alpha G\rho \qquad (3)$$

accounts for pressure-driven flows. The quantity $P^i = \rho T$ is the usual ideal pressure. The presence of the additional term proportional to G gives a compressibility proportional to $T - G$. Hence G measures the deviation from the ideal behaviour of the fluid, being temperature fixed in our simulations. The third term

$$F_\alpha^{\text{interface}} = k\rho \partial_\alpha(\nabla^2 \rho) \qquad (4)$$

represents interfacial forces, with the constant k controlling the surface tension of actin (which controls the width of interfaces between high and low actin densities). The presence of the active component (myosin motors with local density ϕ), and its effects on the fluid, are encoded in the final term

$$F_\alpha^{\text{active}} = \zeta \partial_\alpha \phi, \qquad (5)$$

which accounts for an active isotropic pressure —if $\zeta > 0$ this active pressure is contractile. The parameter ζ measures the strength of myosin-induced contraction. Contractility depends also on the concentration of myosin motors ϕ, which evolves according to the following advection-diffusion equation:

$$\partial_t \phi + \nabla \cdot (\phi \mathbf{v}) = D\nabla^2 \phi - B\nabla^2 \rho - K(\nabla^2)^2 \phi. \qquad (6)$$

Here the local advection velocity of myosin equals that of actin, meaning that all motors are permanently attached to the actomyosin gel. The parameter D is the myosin diffusion coefficient, while K controls the myosin surface tension, quantifying the ability of the myosin droplet to oppose deformation. The term proportional to B is an effective non-equilibrium term, whose effect is to ensure that myosin remains enclosed in actin domains. Higher order gradients terms can in principle be added, but they would not alter the following results. The study is conducted by varying G ("compressibility modulus") and the activity parameter ζ.

The equations of motion are solved by means of a hybrid lattice Boltzmann (LB) scheme, which combines a LB treatment for the Navier-Stokes equation with a finite-difference algorithm to solve the myosin concentration dynamics. The LB solver is implemented by introducing a set of N discrete distribution functions $\{f_i\}$ $(i = 0, \dots, N-1)$ which obey the following dimensionless Boltzmann equation (in the so-called BGK approximation):

$$f_i(\mathbf{r} + \mathbf{e}_i \Delta t, t + \Delta t) - f_i(\mathbf{r}, t) = \\ -\frac{\Delta t}{\tau}[f_i(\mathbf{r}, t) - f_i^{eq}(\mathbf{r}, t)] + \Delta t \mathcal{F}_i, \qquad (7)$$

where $\mathbf{r}$ and t are the spatial coordinates and the time, respectively, $\{\mathbf{e}_i\}$ $(i = 0, \dots, N-1)$ is the set of discrete velocities, Δt is the time step, and τ is a relaxation time which characterizes the relaxation towards the equilibrium distributions f_i^{eq}. The kinematic viscosity ν is related to τ by the relationship $\nu = (\tau - \Delta t/2)$. The value of N depends on the space dimensions and the lattice geometry. We considered a D2Q9 (2D lattice and 9 lattice velocities) geometry and a D3Q15 model for the 3D simulations.

We now briefly describe how we included the important $\mathcal{F}_i$ term in the algorithm. The momenta of the distributions functions define the fluid (actin) density $\rho = \sum_i f_i$ and velocity $\mathbf{u} = \sum_i f_i \mathbf{e}_i / \rho$. The local $\{f_i^{\text{eq}}\}$ $(i = 0, \dots, N-1)$ are expressed by a Maxwell-Boltzmann distribution (MB). Here we adopt a discretization in velocity space of the MB distribution based on the quadrature of a Hermite polynomial expansion of this distribution [15]. In order to simulate the correct transport equations of our nonideal fluid, we follow the approach proposed in [16] to include the forcing term. Within this procedure, the velocity $\mathbf{u}$ is formally replaced by the physical velocity $\tilde{\mathbf{u}}$ given by

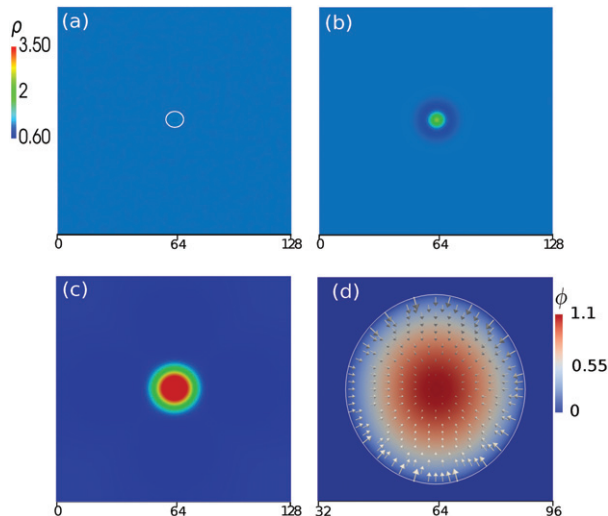$$\rho \tilde{\mathbf{u}} = \sum_i f_i \mathbf{e}_i + \frac{1}{2}\mathbf{F}\Delta t, \qquad (8)$$

---

[1]At least at large times, matrigel can be viewed as a viscous fluid rather than a solid.

Fig. 1: (a)–(c) Snapshots of the evolution of ρ, for a simulation in which ρ has been initialized randomly around 1 (panel (a)), while ϕ as a droplet of radius $R = 3$ (isoline for $\phi = 1$ in panel (a)), for $\zeta = 0.1$ and $G = 0.95$. (d) Contour plot of ϕ with superimposed active force, for the same configuration shown in (c). The isoline for $\rho = 2$ is plotted in white.
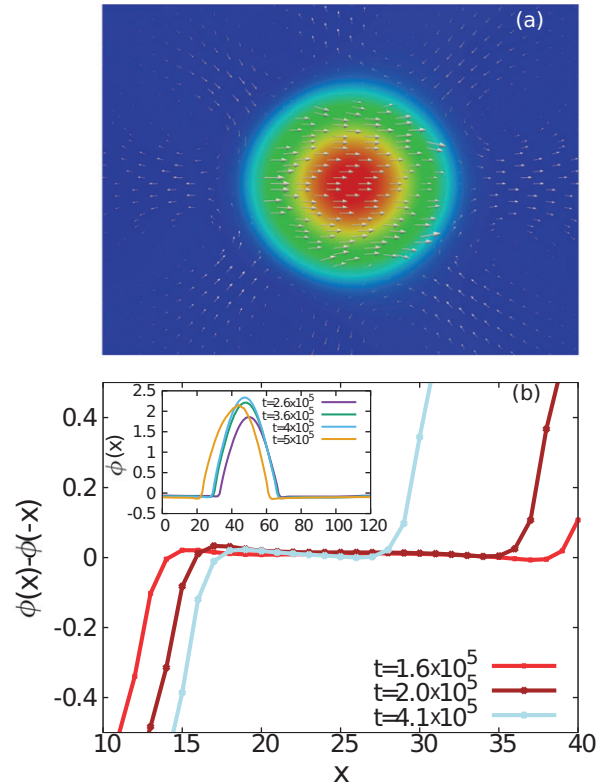

Fig. 2: (a) Contour plot of the density ρ with superimposed velocity field, for $G = 0.88$ and $\zeta = 0.3$. The colour code here is the same of that displayed in fig. 1. (b) main figure: Plot of the quantity $\phi(x) - \phi(-x)$, at different times, and (b) inset: ϕ profiles along the x-direction at different times, for the same case of panel (a). The cyan curve corresponds to the time when the droplet starts moving along the x-direction.

where $\mathbf{F}$ is the total force density acting on the fluid, that is in our case the sum of $\mathbf{F}^{\text{int}}$, $\mathbf{F}^{\text{interface}}$, and $\mathbf{F}^{\text{active}}$. The forcing term in the right end side of eq. (7) is a function of $\mathbf{F}$ and is expressed as a power series at the second-order in the lattice velocities, with coefficients chosen in order to recover eq. (2) in the continuum limit. In all the simulations the lattice space unit $\Delta x = 1$ and $\Delta t = \sqrt{3}/3$ were used to fix the lattice speed $\Delta x/\Delta t = \sqrt{3}$, as prescribed by the Gauss-Hermite quadrature.

The LB solver is coupled with a finite-difference algorithm in order to solve the advection-diffusion equation (eq. (6)). This approach was previously applied to binary mixtures [17], lamellar fluids [18], and active emulsions [19].

Simulations have been performed on a periodic square lattice of size $L = 128$, for the 2D case, and a periodic cubic lattice of size $L = 128$ for 3D simulations. Unless otherwise stated, initial conditions are $\phi = 1$ inside a droplet of radius $R_1 = 3$, and 0 outside , while ρ set equal to $\rho = 1$ inside a droplet of radius $R_2 = 15$, and $\rho = 0.4$ elsewhere. Parameter values are $T = 0.97$, $k = 0.1$, $D = 10^{-3}$, $B = D$, $K = 10^{-3}$. All quantities in the text are reported in lattice (simulation) units.

Results. – We start by presenting the results of our 2D simulations.

The first finding is that contractility alone is able to create a droplet of active fluid (actin, represented by ρ) even in the absence of a free energy favouring phase separation in the passive limit ($\zeta = 0$). Initialising the system with $\rho = \rho_0 + \delta\rho$, where $\rho_0 = 1$ and $\delta\rho$ some small random fluctuations, whereas ϕ (motor concentration) initially set to 1 inside a droplet of radius $R_1 = 3$ and 0

elsewhere, nucleation of a droplet at the centre of the system is observed. Droplet formation occurs for any value of the activity ζ. This clustering phenomenon is due to the interplay between myosin contraction and the cross diffusion term proportional to B in eq. (6), which recruits myosin to regions of high actin concentration. Similar results are obtained with ϕ fluctuating around a uniform value. In all cases, we observe the formation of a single droplet in steady state. Some snapshots of the evolution of the actin density field ρ are reported in fig. 1, together with the steady state contour plots of both ρ and ϕ.

In addition, for every value of the parameter G there is a critical value of activity ζ for which motion occurs. To become motile, the droplet first needs to polarise, breaking the circular symmetry in the myosin distribution. The asymmetry in ϕ can be quantified by analysing the quantity $(\phi(x) - \phi(-x))$, with x a position along a line oriented with the direction of motion, and passing through the centre of mass of the actin droplet. For an isotropic droplet, we expect $(\phi(x) - \phi(-x))$ to be identically zero. Figure 2(b) shows how the myosin field asymmetry develops over time for $G = 0.88$ and $\zeta = 0.3$ (a case for which we have motion). At early times ϕ is nearly
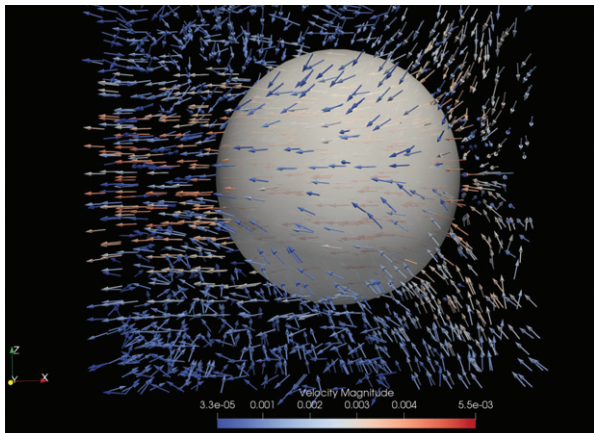
Fig. 3: Isosurface at $\rho = 2$, with superimposed flow field for $\zeta = 0.34$ and $G = 0.87$, in 3D.

symmetric (red curve in the main plot), whereas later myosin redistributes until an asymmetric steady state is reached, and the droplets starts to move (brown curve in the inset of fig. 2(b)).

Figure 2(a) also shows the velocity field of our compressible active system. Inside the droplet, the active contractily driven flows rearrange to give a simple directed flow. There is an opposing flow outside the droplet, which is required for overall momentum conservation (as there are no boundaries or other momentum sinks). The counteracting flow involves a number of vortices which upon azymuthal averaging give a net flow in the direction opposing that of the droplet motion. Whilst vortex patterns are associated with spurious microcurrents in a passive phase-separated systems in LB simulations [20], the magnitude of the flow is over an order of magnitude larger in our active case, and the pattern is different as the vortices in front and behind of the droplet are much larger (we also noted that the spurious passive and the active azymuthal flows are also fitted by different functional forms).

In experiments with cell swimming in a viscous fluid, for instance in a matrigel, the environment is fully 3-dimensional. It is therefore of interest to ask whether contraction-driven flows can rearrange to yield motility in a periodic 3D geometry. To answer this question, we performed simulations in a cubic domain of size $L = 128$. Remarkably, we find that also in 3D droplets —again assembled through myosin-mediated contraction of the compressible actin fluid— become self-motile for sufficiently strong activity. Intriguingly, the solvent flow counteracting droplet motion has now a different form (fig. 3). Two vortex-like structures originate from the poles perpendicular to the migration axis and converge toward the droplet rear, while the outer fluid is pushed away in front of the droplet. This pattern is similar both to that observed experimentally in cells "swimming" in 3D matrigel [12], and to that reported in previous numerical simulations of a self-motile active-liquid crystal droplet [21]. The emergence of this flow patterns is interesting, as our
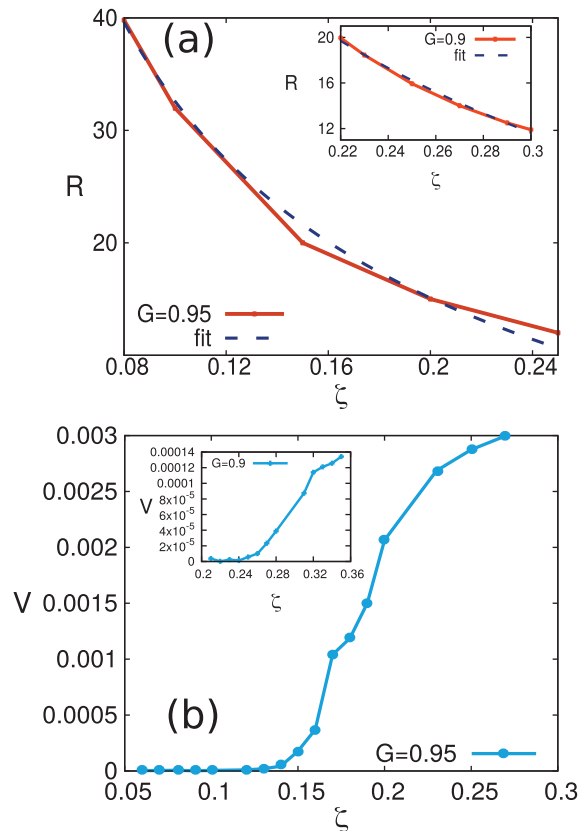

Fig. 4: (a) Critical value of the radius of the droplet R_c as activity varies (continuous curves), for $G = 0.95$ (main figure), and $G = 0.9$ (inset), and the result of the fit (dashed lines) with the proportionality law reported in the text (eq. (9)). (b) Steady state center of mass velocity V as activity varies, for $G = 0.95$ (main figure), and $G = 0.9$ (inset).

model is significantly simpler than the ones previously considered. We interpret the similarity in the flow patterns far from the droplet as due to the fact that the dilute actomyosin background within which the droplet moves may be viewed as an essentially passive viscous polymeric fluid (such as matrigel).

We argue that the mechanism giving rise to the symmetry-breaking instability of a non-motile configuration and ensuring directional motility of a self-propelling cell, is a positive feedback loop, closely related to the one leading to actin accumulation (fig. 1). Here, after *e.g.*, a fluctuation in actin density creates an asymmetry in gradients, the flow generated by contraction is also asymmetrical, and recruits motors faster along the regions where gradients are steeper. This leads to further asymmetric contraction, and to a motile pattern due to the flow imbalance, hence creating an autocatalytic effect [22]. The coupling leads to build motor concentration, which is limited by surface tension and diffusion, resisting the runaway and providing a compensating term which is necessary to achieve a steady state. The droplet breaks symmetry and becomes motile when the activity
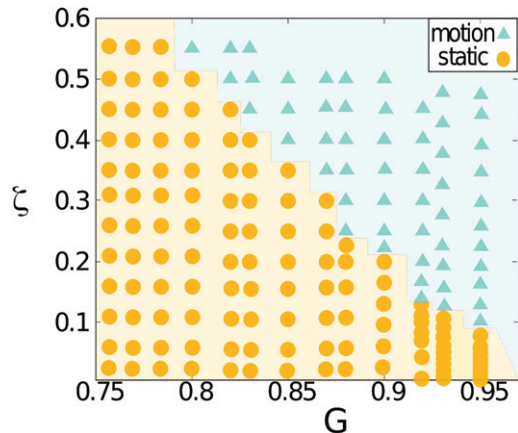
Fig. 5: Phase diagram in the ζ (activity)-G (compressibility) plane, for the transition to motile droplet.

parameter exceeds a threshold. The threshold behaviour originates from the fact that the total myosin stress needs to overcome the effects of actin viscosity and myosin diffusion. Increasing activity for a given value of G, or decreasing G for a given value of ζ, the droplet assumes an accentuated elliptical form.

To understand more quantitatively the effect of the model parameters on the droplet motion, we measured the radius of the self-assembled actin droplet and its velocity in steady state, as a function of the activity parameter ζ, and for different values of the parameter G. The droplet radius at the onset of motion is plotted in fig. 4(a) for two values of G ($G = 0.95$ in the main figure and $G = 0.9$ in the inset). It follows to a good approximation an inverse square root law:

$$R_c \sim \sqrt{\frac{1}{\zeta}}. \qquad (9)$$

Such a dependence was suggested by linear stability analysis of a related problem [7].

Figure 4(b) shows a plot of the center of mass velocity versus ζ for two values of G ($G = 0.95$ in the main figure and $G = 0.9$ in the inset). A phase diagram in the (G, ζ)-plane is instead shown in fig. 5. The steady droplet velocity increases with activity and is bigger for higher values of G. At the same time, decreasing the elastic modulus of the gel —i.e., approaching the incompressible limit $G = 0$— leads to an increase in the activity threshold above which motion is observed. This is consistent with the intuitive expectation that active isotropic contraction cannot lead to motion in this limit (as it is simply equivalent to a redefinition of the pressure). Here for the values of activity ζ we are constrained by the stability of our LB implementation, and for the values of G by the chosen values of T. We checked that fixing T to other values does not change the physical picture discussed, as it solely change the location of the transition line to a motile droplet.

Finally, it is useful to put in relation our parameters choice with the order of magnitude of relevant quantities

measured in real systems. Using $\Delta t = \eta/\zeta_c$ and $\Delta x = \sqrt{D\eta/\zeta_c}$ as time and space units, where ζ_c is a reference value for contractility, it is possible to get the order of magnitude of our model parameters. We set relevant length, time, and viscosity scales for cell extracts and actomyosin droplets as $\Delta t \sim 1\,s$, $\Delta x \sim 1\,\mu m$, and $\eta \sim 10\,\mathrm{Pa\,s}$ [23]. Hence $D \sim 1\,\mu\mathrm{m}^2\mathrm{s}^{-1}$, and $\zeta_c \sim 10\,\mathrm{Pa}$. The former value is close to the *in vivo* myosin diffusion coefficient, while for the latter we note that a myosin concentration of $\phi_0 \sim 1\,\mu\mathrm{M}$ [23], creates a contractility of $\zeta \sim 2\zeta_c$.

Conclusions. – In conclusion, we have shown here that myosin-driven contraction can lead to directed motion within a compressible active fluid. In particular, we have found that within a single compressible actomyosin fluid, the interplay between myosin contraction and cross diffusion is responsible for the self-organization of an actin droplet. Motion requires symmetry breaking, which can arise due to a fluctuation. Once symmetry is broken, a positive feedback mechanism is responsible for the motion. Motors lead to asymmetric contraction, this recruits additional myosin by advection, which reinforces the contraction asymmetry. A steady state is reached because of the competition between this simple positive feedback on one hand, and diffusive and viscous effects on the other hand. Unlike previous work on contraction-driven motility, here we have focused on the effect of compressibility. We have found that compressibility has the effect to facilitate motility, as it decreases the value of the isotropic contractile stress beyond which the droplet starts to move.

We have also shown that the actin flow inside the droplet is a simple and directed one, whereas the counter-acting flow in the compressible solvent has different shapes in 2D and 3D. In 3D, the pattern is reminiscent of that observed experimentally for cell swimming in matrigel. This may be because in steady state the self-assembled droplet swims within a low density actomyosin background which can be approximately viewed as a passive compressible polymeric fluid.

Our results could in principle be directly tested experimentally by studying pattern formation in compressible actomyosin suspensions. They should also be relevant to the physics of cell swimming inside gels with different compressibility.

$$* * *$$

REFERENCES

[1] WEDLICH D., *Cell Migration in Development and Disease* (Wiley) 2006.

[2] PROST J., JOANNY J. F., TURLIER H. and AUDOLY B., *Biophys. J.*, **106** (2014) 114.

[3] ALLEN G. M., THERIOT J. A., BARNHART E., LEE K. C. and MOGILNER A., *Proc. Natl. Acad. Sci. U.S.A.*, **112** (2015) 5045.

[4] DESIMONE A. and GIOMI L., *Phys. Rev. Lett.*, **112** (2014) 147802.

[5] TJHUNG E., MARENDUZZO D. and CATES M. E., *Proc. Natl. Acad. Sci. U.S.A.*, **109** (2012) 12381.

[6] RECHO P., PUTELAT T. and TRUSKINOVSKY L., *Phys. Rev. Lett.*, **111** (2013) 108102.

[7] LE GOFF T., LIEBCHEN B. and MARENDUZZO D., *Acto-myosin contraction induces droplet motility*, arXiv:1712.03138 (2003).

[8] BRAY D., *Cell Movements: From Molecules to Motility* (Garland Pub.) 2001.

[9] PHILLIPS R. B., KONDEV J. and THERIOT J., *Physical Biology of the Cell* (Garland Science) 2009.

[10] BARNHART E., LEE C., KEREN K., MOGILNER A. and THERIOT J. A., *PLOS Biol.*, **9** (2011) e1001059.

[11] LE GOFF T., LIEBCHEN B. and MARENDUZZO D., *Phys. Rev. Lett.*, **117** (2016) 238002.

[12] POINCLOUX R., COLLIN O., LIZARRAGA F., ROMAO M., DEBRAY M., PIEL M. and CHAVRIER P., *Proc. Natl. Acad. Sci. U.S.A.*, **108** (2011) 1943.

[13] KELLER H., ZADEH A. D. and EGGLI P., *Cell Motil. Cytoskelet.*, **53** (2002) 189.

[14] DE MAGISTRIS G., TIRIBOCCHI A., WHITFIELD C. A., HAWKINS R. J., CATES M. E. and MARENDUZZO D., *Soft Matter*, **10** (2014) 7826.

[15] SHAN X., YUAN X. F. and CHEN H., *J. Fluid Mech.*, **550** (2006) 413.

[16] TIRIBOCCHI A., STELLA N., GONNELLA G. and LAMURA A., *Phys. Rev. E*, **80** (2009) 026701.

[17] GUO Z., ZHENG C. and SHI B., *Phys. Rev. E*, **65** (2002) 046308.

[18] GONNELLA G., LAMURA A. and TIRIBOCCHI A., *Philos. Trans. R. Soc. A*, **369** (2011) 2592.

[19] NEGRO G., CARENZA L. N., DIGREGORIO P., GONNELLA G. and LAMURA A., *Phys. A: Stat. Mech. Appl.*, **503** (2018) 464.

[20] WAGNER A. J., *Int. J. Mod. Phys. B*, **17** (2003) 193.

[21] TJHUNG E., TIRIBOCCHI A., MARENDUZZO D. and CATES M. E., *Nat. Commun.*, **6** (2015) 5420.

[22] MAYER M., DEPKEN M., BOIS J. S., JÜLICHER F. and GRILL S., *Nature*, **467** (2010) 617.

[23] NORSTROM M. and GARDEL M. L., *Soft Matter*, **7** (2011) 3228.